Cold sprayed FeCoNiCrMn High Entropy Alloy (HEA) coating: microstructure and tribological property

Shuo Yin, Rocco Lupoi
Trinity College Dublin, The University of Dublin, Department of Mechanical & Manufacturing Engineering, Parsons Building, Dublin 2, Ireland
lupoir@tcd.ie ; yins@tcd.ie

Wenya Li, Yaxin Xu
Key Laboratory of Solidification Processing, Shaanxi Key Laboratory of Friction Welding Technologies, School of Materials Science and Engineering, Northwestern Polytechnical University, Xi'an 710072, PR China
liwy@nwpu.edu.cn

Bo Song
Key Laboratory of Materials Processing and Die & Mould Technology, Huazhong University of Science and Technology, Wuhan 430074, PR China

Xingchen Yan, Min Kuang
National Engineering Laboratory for Modern Materials Surface Engineering Technology; The Key Lab of Guangdong for Modern Surface Engineering Technology; Guangdong Institute of New Materials, Guangzhou 510651, P.R. China

Abstract

High entropy alloys (HEAs) are of great interest in the community of materials science and engineering due to their unique phase structure. They are constructed with five or more principal alloying elements in equimolar or near-equimolar ratios. Therefore, HEAs can derive their performance from multiple principal elements rather than a single element. In this work, solid-state cold spraying (CS) was applied for the first time to produce a FeCoNiCrMn HEA coating, and also mixed with Al_2O_3 in a separate experiment. The experimental results confirm that CS can be used to produce a thick HEA coating with low porosity. As a low-temperature deposition process, CS completely retained the HEA phase structure in the coating without any phase transformation. The characterization also reveals that the grains in the CSed HEA coating had experienced significant refinement as compared to those in the as-received HEA powder due the occurrence of dynamic recrystallization at the highly deformed interparticle region. Due to the increased dislocation density and grain boundaries, CSed HEA coating was much harder than the as-received powder. The tribological study shows that the CSed FeCoNiCrMn HEA coating resulted in lower wear rate than laser cladded HEA coatings.

Introduction

High entropy alloys (HEAs) are new member of the metal alloy family. They are constructed with five or more principal alloying elements in equimolar or near-equimolar ratio, and thus derive their performances from multiple principal elements rather than a single element [1,2]. Due to their unique phase structure, HEAs have superior mechanical properties, corrosion-resistance performance, wear-resistance performance, oxidation-resistance performance and many other advantages as compared to conventional alloys [3,4]. They have attracted high interest from both scientific and industrial communities. Coatings can provide effective protection to the underlying materials against aggressive environments such as severe wear, severe corrosion, and high temperature. It is considered that HEAs are great candidates for coating materials due to their superior properties over conventional metals. Hence, HEA coatings have been investigated in recent years. Currently, HEA coatings were mainly produced using fusion-based technologies, such as laser cladding [5–12], plasma cladding [13–15], plasma spraying [16–20] and magnetron sputtering [21–26]. However, melting and solidification frequently result in phase transformation and element segregation of the HEA coatings, breaking the nature of HEAs [27–29]. Therefore, it is important to find a non-fusion-based coating technology to prevent the phase transformation of HEAs during coating formation.

Cold spraying (CS) is a solid-state coating deposition technology developed in the 1980s; the powder feedstock remains solid state during the entire deposition process [30–33]. As shown in Fig. 1, in this process, compressed gases (typically nitrogen and helium) are used as the propulsive gas to accelerate powder feedstock (typically metals) to a high velocity in a de Laval type nozzle and to induce deposition when the powders impact onto a substrate (typically metals) at a velocity over a critical value. In contrast to the conventional fusion-based coating deposition processes, the formation of CSed coatings relies largely on the particle kinetic energy rather than thermal energy. Deposition is achieved through local metallurgical bonding at the interparticle and coating/substrate interfaces. Due to the low processing temperature, CS allows for the avoidance of defects commonly encountered in high-temperature deposition processes, such as oxidation, residual thermal stress and phase transformation. Therefore, CS has been successfully used to

deposit various metal-based materials including metals, alloys and metal matrix composites (MMCs) [34–36], showing potentials in producing HEA coatings.

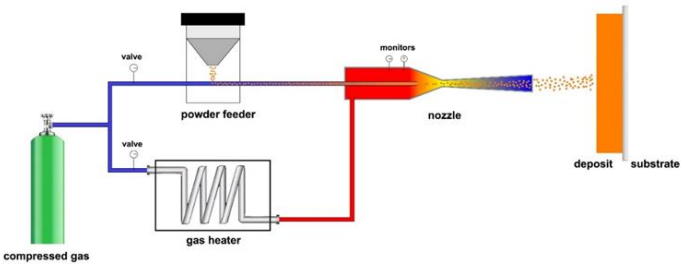

Figure 1: Schematic of a CS system and its working principle.

In this paper, CS was used for the first time to produce the HEA coating. FeCoNiCrMn HEA powder was used as the feedstock, and helium, which can enhance the HEA particle plastic deformation and deposition, was used as the propulsive gas. Various characterization methods were applied to characterize the coating microstructure, phase composition and tribological properties. In addition, HEA-Al_2O_3 MMC coating was also produced, and its tribological property was investigated and compared to the pure HEA coating.

Experimental methodology

Fabrication of the HEA coating with CS

Spherical FeCoNiCrMn HEA powder (Vilory Advanced Materials Technology Ltd, China) with a size range between 15 and 53 μm was selected as the feedstock. Fig. 2 shows the morphology of the HEA powder observed by scanning electron microscope (SEM, Carl Zeiss Ultra Plus, Germany), where dendritic grain structure can be clearly observed. The nominal composition of the HEA powder is provided in Table 1. The HEA-based MMC coating was produced using Al_2O_3 particles (−75+53 μm, Kuhmichel, Germany) as reinforcements. The HEA-Al_2O_3 mixing powder was prepared through mechanical blending at the ratio of 80 vol.% for HEA to vol. 20% for Al_2O_3. The coatings were deposited on a flat 6028 Al alloy substrate under 4 nozzle passes using an in-house CS system (Trinity College Dublin, Ireland). The system consists of high pressure propulsive gas stored in cylinders, gas heater, powder feeder, computer control working platform for controlling the substrate movement, de-Laval nozzle and computer control unit for spray system. The nozzle used in this work has a round cross-sectional shape with a divergent length of 180mm. The throat and outlet diameters are 2 mm and 6 mm, respectively. Compressed helium was used as the propulsive gas with the inlet pressure and temperature of 3.0 MPa and 300 °C, respectively. The standoff distance from the nozzle exit to the substrate surface and the nozzle traverse speed were 30 mm and 100 mm/s, respectively. In order to study the coating/substrate bonding mechanism, single HEA particle impact test was also carried out at a high gun traversal speed of 300 mm/s.

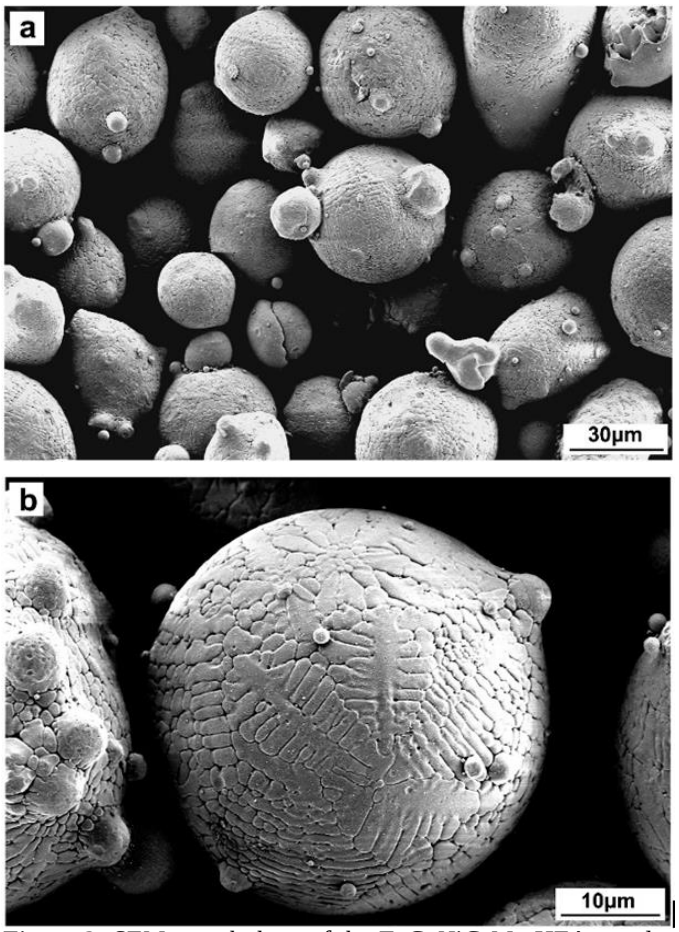

Figure 2: SEM morphology of the FeCoNiCrMn HEA powder used in this work. (a) overall view, and (b) magnified view of a single HEA particle.

Table 1: Nominal composition of the FeCoNiCrMn HEA powder used in this work.

Element	Fe	Co	Ni	Cr	Mn
wt. %	20.09	20.96	21.01	18.86	Bal.

Materials characterization

In order to examine the phase composition of the CSed HEA coating, the coating sample was examined by an X-Ray diffractometer (XRD, Siemens D500, Germany) with the Co (λ=1.789 Å) source at a current of 40 mA, voltage of 35 kV and scan step of 0.02°. In order to assess the coating microstructure via SEM, the cross-sectional samples were prepared using standard metallographic procedures with the final polishing applied by 0.06 μm colloidal silica. The element analysis of the HEA powder and coating was performed using an energy-dispersive X-ray spectroscopy (EDX) unit (Oxford Instruments AZtec, UK) equipping on the SEM system. The grain structures of the HEA powder and coating were characterized by using electron backscatter diffraction (EBSD) equipping on the SEM system. The porosity of the HEA coating and the volume content and size

of the Al_2O_3 reinforcements in the HEA-Al_2O_3 MMC coating were evaluated based on binary image analysis using ImageJ software. The microhardness of the HEA powder and coating was tested using a Vickers hardness indenter (Mitutoyo, Japan) with a load of 100 g and dwell time of 10 s. Ten locations were tested on each sample, and the average value was considered the sample microhardness.

Tribological test

The tribological property of the CSed coatings was measured using POD-2 pin-on-disc tribometer (CSEM Instruments, Switzerland) at room temperature. For the accurate measurement of wear rate, the sample surfaces were polished using silicon carbide first, followed by 6 μm diamond solution prior to the test, and the samples were then mounted on a carrier disc. A WC ball with a diameter of 5 mm was used as the counterpart under a constant load of 5 N. The disk rotated at a linear speed of 10 mm/s. The material volume loss was calculated according to ASTM G 99 standard [43]. The wear rate was calculated as the volume loss per unit load per traverse distance. The sliding distance and track diameter were 200m and 5mm, respectively.

Results and discussion

Phase composition and microstructure

Fig. 3a shows the photo of the CSed HEA coating after machining into a cubic shape with a surface area of 20 mm × 20 mm and coating thickness of 1.5 mm. The phase composition and microstructure characterization of the HEA coating is shown in Fig. 3b and c. The XRD spectra shown in Fig. 3b reveals that both the HEA powder and HEA coating had only fcc single phase. Due to the low processing temperature, no evidence of phase change and oxidation were observed in the HEA coating. This is a unique advantage of CS over other thermal spray processes. In addition, the peak detected in the HEA coating was slightly boarder than that in the HEA powder, indicating the possible occurrence of grain refinement in the coating, which will be discussed in detail in the following section. Fig. 3c shows the cross-sectional image of the CSed HEA coating. As can be seen, the HEA coating was rather dense with a porosity of 0.47±0.17%, which is much lower than that of plasma sprayed HEA coatings (7.4±1.3%) [37]. At the coating/substrate interface, 'interlocking' phenomenon in the form of coating material mechanically trapped by the substrate material was observed. The formation of the 'interlocking' was due to the severe plastic deformation of the soft Al alloy substrate upon impact by the hard HEA particles, which is shown by Fig. 4 where a single HEA particle was completely locked by the highly deformed substrate material. Such 'interlocking' can provide high adhesive strength to the coating/substrate interface.

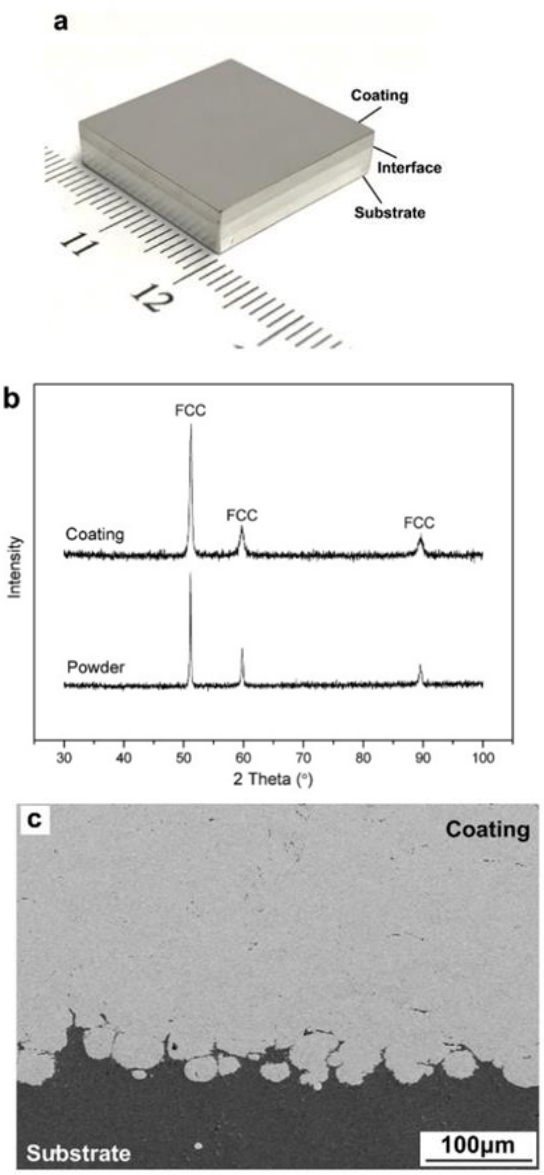

Figure 3: General characterization of the CSed HEA coating. (a) photo of the HEA coating machined after spraying, (b) XRD spectra of the HEA powder and coating, and (c) cross-sectional SEM image of the HEA coating.

For further understanding the microstructure of the CSed HEA coating, Fig. 5a shows the high-resolution SEM image of the CSed HEA coating cross-section. Interparticle interfaces as marked by black arrows could be observed, which arose from the insufficient local plastic deformation. Being weak points, the interparticle interfaces are not favorable to the coating cohesion strength and properties [32]. However, they can be mitigated through adjusting the deposition parameters (e.g., increasing the gas pressure and temperature, applying powder preheating) or post-spray annealing [32]. Fig. 5b shows the EDX mapping of the HEA coating acquired at the selected area marked in Fig. 5a. It is clearly seen from the EDX map that five elements uniformly distributed in the coating without obvious segregation and inter-reaction, which further proves that the low-temperature CS process can effectively prevent the phase change of HEA powder.

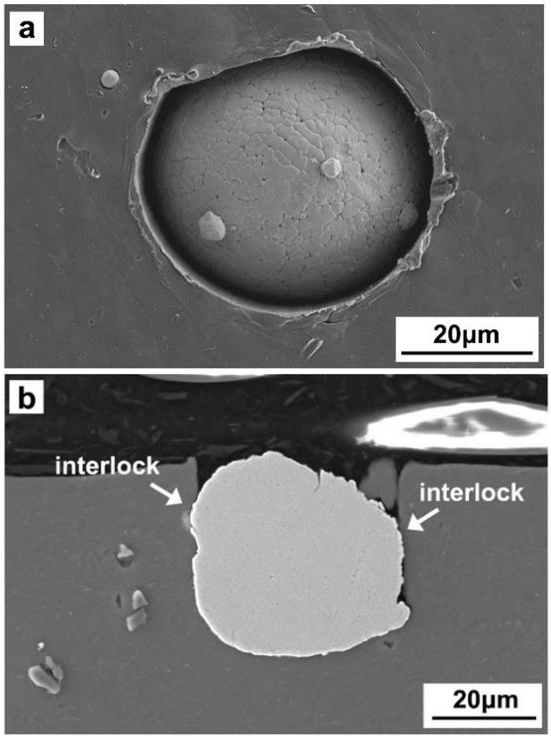

Figure 4: Characterization of a single HEA particle depositing onto a 6028 Al alloy substrate. (a) Surface morphology and (b) cross-sectional view.

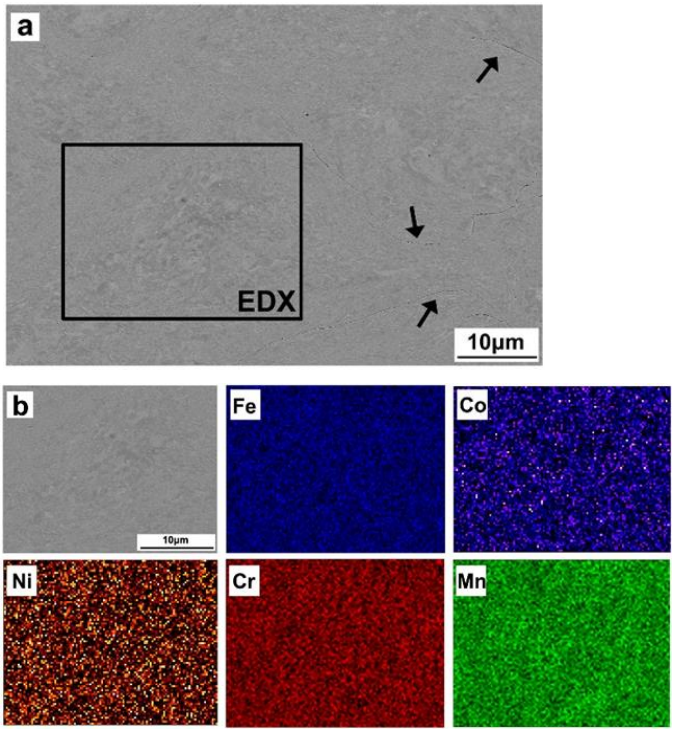

Figure 5: (a) Cross-sectional SEM image of the CSed HEA coating in high magnification and (b) EDX map acquired at the selected area marked in Fig. 5a.

Grain structure

EBSD characterization was performed to reveal the grain structure of the CSed HEA coating. Fig. 6 shows the inverse pole figures (IPFs) of a single HEA powder and the CSed HEA coating at their cross-sections. It is clear that CS processing caused significant refinement of HEA grains. As addressed in Section 3.1, in CS, particles undergo severe plastic deformation upon impact with deposited coating. Together with the high strain/strain-rate plastic deformation, significant dislocation multiplication, dislocation density increase and dislocation accumulation occur within the interparticle interfaces, resulting in the formation of dislocation cells and thus refinement of coarse grains into subgrains. At the localized interparticle interfacial regions where the particle material has experienced the largest plastic deformation, dynamic recrystallization occurs under the combined action of adiabatic heating and plastic deformation, leading to a further refinement of subgrains into ultrafine grains [38–43]. These are the reasons why the HEA grains in the CSed coating were significantly refined compared to those in the as-received powder. The increased dislocation density and the number of grain boundaries contributed together to the hardening effect, resulting in a considerable increase of the microhardness of the HEA from 124.01+38.92 Hv in powder state by three times to 332.91+34.74 Hv in coating state after CS.

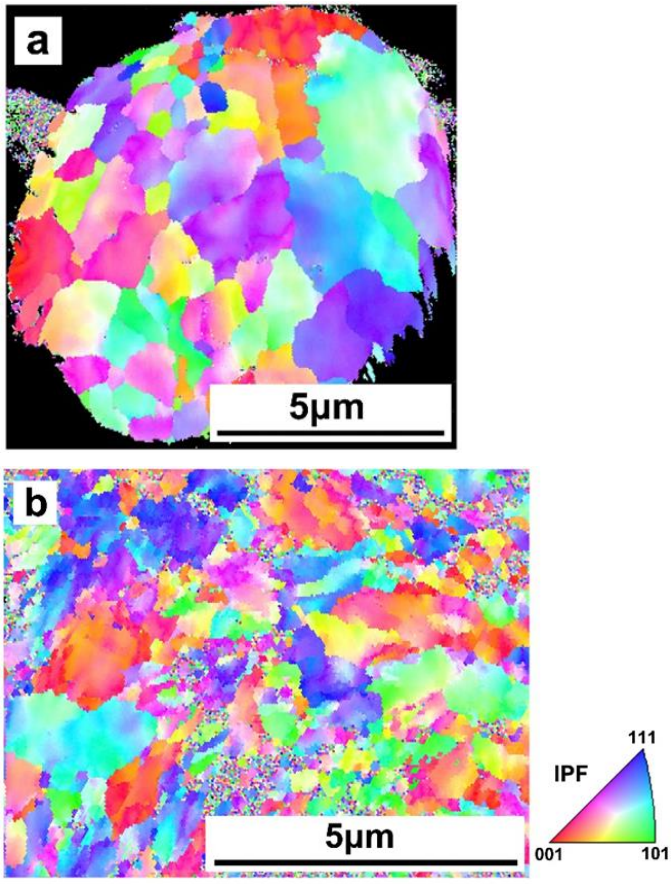

Figure 6: EBSD IPF maps of (a) a single HEA particle and (b) the CSed HEA coating.

HEA-Al_2O_3 MMC coating

CSed MMC coatings have shown improved properties as compared to pure metal coatings [44]. Fig. 7a shows the cross-sectional image of the CSed HEA-Al_2O_3 MMC coating; the inserted figure illustrates the photo of the machined coating sample. As can be seen, the HEA-Al_2O_3 MMC coating was rather thick with the Al_2O_3 reinforcements uniformly dispersed in the HEA matrix. The volume content of the Al_2O_3 reinforcements in the MMC coating was measured as 4.89 ± 0.49%, which is much lower than that in the mixing powder (20%). This phenomenon suggests that most of the Al_2O_3 particles failed the deposition upon impact during CS due to the lack of metallurgical bonding with the HEA matrix phase [45]. In addition, the average size of the Al_2O_3 reinforcements in the MMC coating was 26.73 ± 4.56 μm which is much smaller than the original powder size (−75+53 μm), indicating that Al_2O_3 particles severely fractured into fragments upon impact. Most of the fragments rebounded after impact and only a small part could deposit. This is another reason why the content of Al_2O_3 in the coating was lower. The coating/substrate interface shown in Fig. 7b reveals the formation of 'interlocking', which is similar to the interface shown in Fig. 3c.

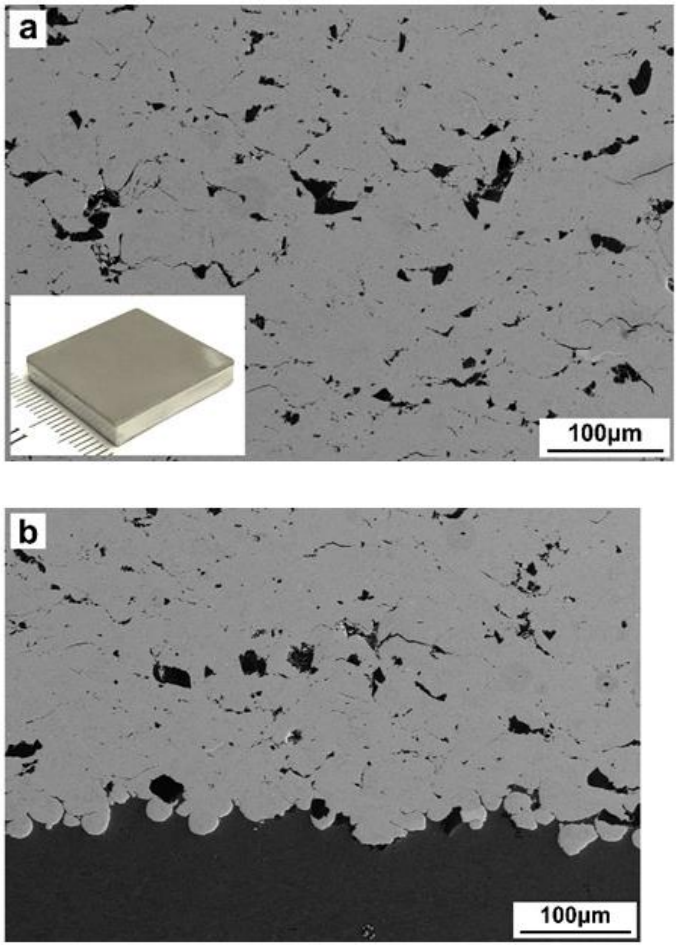

Figure 7: Cross-sectional image of (a) the CSed HEA-Al_2O_3 coating with 20 vol.% Al_2O_3 in the premixed powder and (b) the coating/substrate interface.

Tribological property

The tribological property of the CSed HEA coating was studied and compared to the HEA coatings produced via laser cladding.

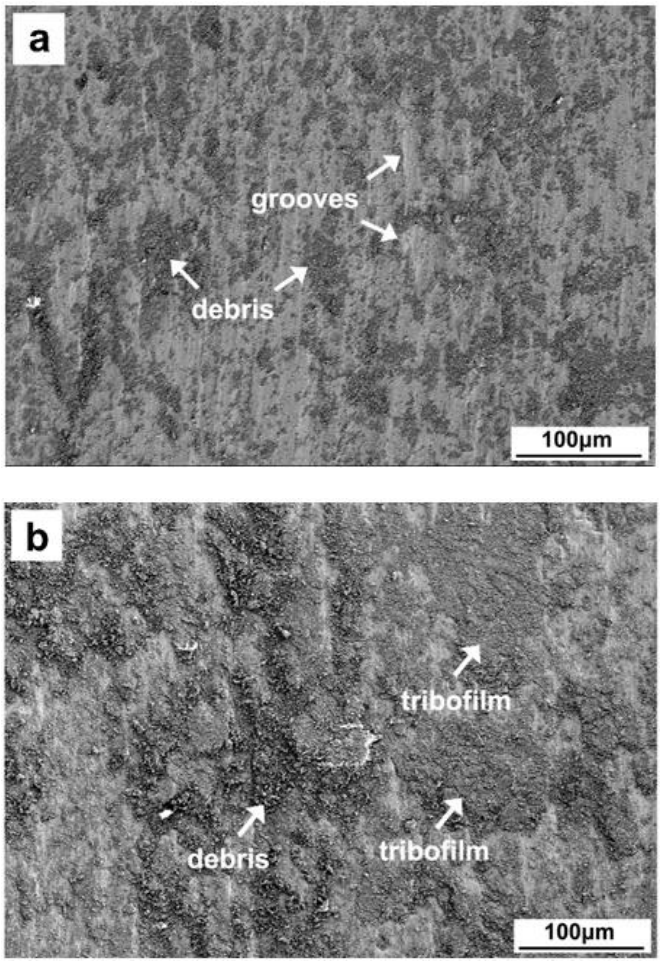

Figure 8: Worn surfaces of (a) the CSed HEA coating and (b) the CSed HEA-AlO_3 MMC coating.

After sliding test, the CSed HEA coating resulted in a wear rate of $4.76\pm0.22\times10^{-4}$ $mm^3/N\cdot m$, which is lower than the laser cladded CoCrBFeNiSi and FeCoCrBNiSi HEA coatings [8,46]. The reason for this could be the work-hardening effect during CS deposition which significantly increases the hardness of the CSed HEA coating. Fig. 8a shows the worn surface of the CSed HEA coating. It is seen that the worn surface was characterized by microgrooves and fragmented HEA debris, indicating that the HEA coating experienced deformation and material peel-off during the sliding test, which are typical features of abrasion wear [47,48]. The sliding test on the CSed HEA-Al_2O_3 MMC coating shows that the MMC coating resulted in a wear rate of $2.41\pm0.68\times10^{-4}$ $mm^3/N\cdot m$, approximately 50% lower as compared to the CSed pure HEA coating ($4.76\pm0.22\times10^{-4}$ $mm^3/N\cdot m$), showing significant improvement in wear resistance. Fig. 8b shows the worn surface of the HEA-Al_2O_3 MMC coating. Discontinuous strain-hardened tribofilms and debris were formed on the worn surface, which indicates that the wear mechanism changed

from abrasion for the CSed HEA coating to adhesion for CSed HEA-Al_2O_3 MMC coating. The tribofilm prevented the direct contact between the coating material and the pin ball, protecting the underlying coating surface from further wear [34,49]. Therefore, the HEA-Al_2O_3 MMC coatings resulted in lower wear rate than the pure HEA coating.

Conclusions

In this work, solid-state cold spray technology was applied to produce FeCoNiCrMn HEA coating and HEA-Al_2O_3 MMC coating. The HEA coating produced with CS had very low porosity and completely retained the HEA phase structure without any phase transformation. The grain structure of the CSed HEA coating was significantly refined as compared to that in the as-received HEA powder due the increased dislocation density and occurrence of dynamic recrystallization. Therefore, the CSed HEA coating was much harder than the as-received HEA powder. In addition to the pure HEA coating, HEA-Al_2O_3 MMC coating was also produced via CS. The experimental results indicate that the Al_2O_3 particles suffered from severe fracture during the deposition but uniformly distributed within the HEA matrix. Due to the lack of metallurgical bonding with the HEA matrix, the HEA particles tended to rebound after impact, resulting in lower content in the MMC coating than in the premixed powder. The tribological study shows that the CSed HEA coating resulted in lower wear rate than laser cladded HEA coatings. The CSed HEA-Al_2O_3 MMC coating resulted in even better wear resistance than the CSed pure HEA coating. This work for the first time proves that solid-state CS technology is promising for the fabrication of thick and dense HEA and HEA-Al_2O_3 coatings. Further in-depth investigations are encouraged to fully understand the microstructure and properties of CSed HEA and CSed-Al_2O_3 coatings.

Acknowledgments

The authors would like to thank the financial support from Irish Research Council project GOIPD-2017-912 and the European Space Agency (4000112844/14/NL/FE). We also thank the CRANN Advanced Microscopy Laboratory in Trinity College Dublin for the support in data analysis.

References

1. J.W. Yeh, *et al.*, Nanostructured high-entropy alloys with multiple principal elements: Novel alloy design concepts and outcomes, *Adv. Eng. Mater*. 6 (2004) 299–303+274. doi:10.1002/adem.200300567.
2. D.B. Miracle, O.N. Senkov, A critical review of high entropy alloys and related concepts, *Acta Mater*. 122 (2017) 448–511. doi:10.1016/j.actamat.2016.08.081.
3. Y. Zhang, *et al.*, Microstructures and properties of high-entropy alloys, Prog. Mater. Sci. 61 (2014) 1–93. doi:10.1016/j.pmatsci.2013.10.001.
4. Y.F. Ye, *et al.*, High-entropy alloy: challenges and prospects, *Mater. Today.* 19 (2016) 349–362. doi:10.1016/j.mattod.2015.11.026.
5. G. Jin, *et al*., D. zhang, High temperature wear performance of laser-cladded FeNiCoAlCu high-entropy alloy coating, *Appl. Surf. Sci*. 445 (2018) 113–122. doi:10.1016/j.apsusc.2018.03.135.
6. F.Y. Shu, *et al*., Structure and high-temperature property of amorphous composite coating synthesized by laser cladding FeCrCoNiSiB high-entropy alloy powder, *J. Alloys Compd.* 731 (2018) 662–666. doi:10.1016/j.jallcom.2017.08.248.
7. Y. Cai, *et al*., Influence of dilution rate on the microstructure and properties of FeCrCoNi high-entropy alloy coating, *Mater. Des.* 142 (2018) 124–137. doi:10.1016/j.matdes.2018.01.007.
8. F.Y. Shu, *et al*., Microstructure and high-temperature wear mechanism of laser cladded CoCrBFeNiSi high-entropy alloy amorphous coating, *Mater. Lett*. 211 (2018) 235–238. doi:10.1016/j.matlet.2017.09.056.
9. Z. Cai, *et al*., Microstructure and wear resistance of laser cladded Ni-Cr-Co-Ti-V high-entropy alloy coating after laser remelting processing, *Opt. Laser Technol*. 99 (2018) 276–281. doi:10.1016/j.optlastec.2017.09.012.
10. N. Ley, *et al*., Laser coating of a CrMoTaWZr complex concentrated alloy onto a H13 tool steel die head, *Surf. Coatings Technol*. 348 (2018) 150–158. doi:10.1016/j.surfcoat.2018.02.038.
11. Q. Ye, *et al.*, Microstructure and corrosion properties of CrMnFeCoNi high entropy alloy coating, *Appl. Surf. Sci.* 396 (2017) 1420–1426. doi:10.1016/j.apsusc.2016.11.176.
12. C.L. Wu, *et al.*, Phase evolution and cavitation erosion-corrosion behavior of FeCoCrAlNiTixhigh entropy alloy coatings on 304 stainless steel by laser surface alloying, *J. Alloys Compd*. 698 (2017) 761–770. doi:10.1016/j.jallcom.2016.12.196.
13. J. Lu, *et al.*, Microstructure evolution and properties of CrCuFexNiTi high-entropy alloy coating by plasma cladding on Q235, *Surf. Coatings Technol*. 328 (2017) 313–318. doi:10.1016/j.surfcoat.2017.08.019.
14. Z. Cai, *et al*., Design and microstructure characterization of FeCoNiAlCu high-entropy alloy coating by plasma cladding: In comparison with thermodynamic calculation, *Surf. Coatings Technol*. 330 (2017) 163–169. doi:10.1016/j.surfcoat.2017.09.083.
15. J.B. Cheng, X.B. Liang, B.S. Xu, Effect of Nb addition on the structure and mechanical behaviors of CoCrCuFeNi high-entropy alloy coatings, Surf. Coatings Technol. 240 (2014) 184–190. doi:10.1016/j.surfcoat.2013.12.053.
16. B. Jin, *et al.*, Microstructure and properties of laser re-melting FeCoCrNiAl0.5Sixhigh-entropy alloy

coatings, *Surf. Coatings Technol*. 349 (2018) 867–873. doi:10.1016/j.surfcoat.2018.06.032.
17. W.L. Hsu, *et al.*, On the study of thermal-sprayed Ni0.2Co0.6Fe0.2CrSi0.2AlTi0.2HEA overlay coating, Surf. Coatings Technol. 316 (2017) 71–74. doi:10.1016/j.surfcoat.2017.02.073.
18. W.L. Hsu, et al., Thermal sprayed high-entropy NiCo0.6Fe0.2Cr1.5SiAlTi0.2coating with improved mechanical properties and oxidation resistance, *Intermetallics*. 89 (2017) 105–110. doi:10.1016/j.intermet.2017.05.015.
19. D.Y. Lin, *et al*., Influence of laser re-melting and vacuum heat treatment on plasma-sprayed FeCoCrNiAl alloy coatings, *J. Iron Steel Res. Int*. 24 (2017) 1199–1205. doi:10.1016/S1006-706X(18)30018-9.
20. L.M. Wang, *et al.*, The microstructure and strengthening mechanism of thermal spray coating NixCo0.6Fe0.2CrySizAlTi0.2high-entropy alloys, *Mater. Chem. Phys.* 126 (2011) 880–885. doi:10.1016/j.matchemphys.2010.12.022.
21. W. Zhang, *et al.*, Preparation, structure, and properties of an AlCrMoNbZr high-entropy alloy coating for accident-tolerant fuel cladding, *Surf. Coatings Technol.* 347 (2018) 13–19. doi:10.1016/j.surfcoat.2018.04.037.
22. F. Cao, P. Munroe, Z. Zhou, Z. Xie, Microstructure and mechanical properties of a multilayered CoCrNi/Ti coating with varying crystal structure, *Surf. Coatings Technol.* 350 (2018) 596–602. doi:10.1016/j.surfcoat.2018.07.066.
23. Z. Chang, Structure and properties of duodenary (TiVCrZrNbMoHfTaWAlSi) N coatings by reactive magnetron sputtering, *Mater. Chem. Phys.* 220 (2018) 98–110. doi:10.1016/j.matchemphys.2018.08.068.
24. M.A. Tunes, V.M. Vishnyakov, S.E. Donnelly, Synthesis and characterisation of high-entropy alloy thin films as candidates for coating nuclear fuel cladding alloys, *Thin Solid Films*. 649 (2018) 115–120. doi:10.1016/j.tsf.2018.01.041.
25. W. Liao, *et al*., Nanocrystalline high-entropy alloy (CoCrFeNiAl0.3) thin-film coating by magnetron sputtering, *Thin Solid Films.* 638 (2017) 383–388. doi:10.1016/j.tsf.2017.08.006.
26. Z.F. Wu, *et al.*, Microstructure characterization of AlxCo1Cr1Cu1Fe1Ni1(x = 0 and 2.5) high-entropy alloy films, *J. Alloys Compd*. 609 (2014) 137–142. doi:10.1016/j.jallcom.2014.04.094.
27. Z. Cai, *et al.*, TEM observation on phase separation and interfaces of laser surface alloyed high-entropy alloy coating, *Micron.* 103 (2017) 84–89. doi:10.1016/j.micron.2017.10.001.
28. Z. Cai, *et al*., Synthesis and microstructure characterization of Ni-Cr-Co-Ti-V-Al high entropy alloy coating on Ti-6Al-4V substrate by laser surface alloying, *Mater. Charact.* 120 (2016) 229–233. doi:10.1016/j.matchar.2016.09.011.
29. Z. Cai, *et al*., In situ TEM tensile testing on high-entropy alloy coating by laser surface alloying, *J. Alloys Compd.* 708 (2017) 380–384. doi:10.1016/j.jallcom.2017.03.049.
30. A.P.Alkhimov, V.F. Kosarev, N.I. Nesterovich, A.N. Papyrin., Method of applying coatings (SU 1618778), 1980.
31. A.P. Alkhimov, V.F. Kosareve, A.N. Papyrin, A Method of Cold Gas-Dynamic Spray Deposition, *Dokl. Akad. Nauk SSSR.* 315 (1990) 1062–1065.
32. S. Yin, *et al.*, Cold spray additive manufacturing and repair: Fundamentals and applications, *Addit. Manuf*. 21 (2018) 628–650. doi:10.1016/j.addma.2018.04.017.
33. W. Li, et al., Solid-state additive manufacturing and repairing by cold spraying: A review, *J. Mater. Sci.* Technol. 34 (2018) 440–457. doi:10.1016/j.jmst.2017.09.015.
34. C. Huang, *et al.*, Effect of Substrate Type on Deposition Behavior and Wear Performance of Ni-Coated Graphite/Al Composite Coatings Deposited by Cold Spraying, *J. Mater. Sci. Technol.* 33 (2017) 338–346. doi:10.1016/j.jmst.2016.11.016.
35. R. Jenkins, *et al.*, New insights into the in-process densification mechanism of cold spray Al coatings: low deposition efficiency induced densification, J. *Mater. Sci. Technol.* (2018). doi:10.1016/j.jmst.2018.09.045.
36. K. Yang, et al., Characterizations and anisotropy of cold-spraying additive-manufactured copper bulk, J. Mater. Sci. Technol. 34 (2018) 1570–1579. doi:10.1016/j.jmst.2018.01.002.
37. A.S.M. Ang, *et al.*, Plasma-Sprayed High Entropy Alloys: Microstructure and Properties of AlCoCrFeNi and MnCoCrFeNi, Metall. Mater. Trans. A Phys. *Metall. Mater. Sci.* 46 (2014) 791–800. doi:10.1007/s11661-014-2644-z.
38. K. Kim, *et al.*, Grain refinement in a single titanium powder particle impacted at high velocity, *Scr. Mater.* 59 (2008) 768–771. doi:10.1016/j.scriptamat.2008.06.020.
39. K. Kim, M. Watanabe, S. Kuroda, Thermal softening effect on the deposition efficiency and microstructure of warm sprayed metallic powder, *Scr. Mater*. 60 (2009) 710–713. doi:10.1016/j.scriptamat.2008.12.050.
40. M.R. Rokni, C.A. Widener, V.R. Champagne, Microstructural evolution of 6061 aluminum gas-atomized powder and high-pressure cold-sprayed deposition, *J. Therm. Spray Technol.* 23 (2014) 514–524. doi:10.1007/s11666-013-0049-y.
41. K. Kang, *et al.*, Microstructure and texture of Al coating during kinetic spraying and heat treatment, *J. Mater. Sci*. 47 (2012) 4053–4061. doi:10.1007/s10853-012-6259-8.
42. P.C. King, S.H. Zahiri, M. Jahedi, Microstructural refinement within a cold-sprayed copper particle, *Metall. Mater. Trans.* 40 (2009) 2115–2123. doi:10.1007/s11661-009-9882-5.
43. H. Assadi, *et al.*, Bonding mechanism in cold gas spraying, *Acta Mater.* 51 (2003) 4379–4394. doi:10.1016/S1359-6454(03)00274-X.

44. S. Yin, *et al.*, Advanced diamond-reinforced metal matrix composites via cold spray: Properties and deposition mechanism, *Compos. Part B Eng*. 113 (2017) 44–54. doi:10.1016/j.compositesb.2017.01.009.
45. W. Li, *et al.*, A Review of Advanced Composite and Nanostructured Coatings by Solid-State Cold Spraying Process, *Crit. Rev. Solid State Mater. Sci.* 8436 (2018). doi:10.1080/10408436.2017.1410778.
46. F. Shu, *et al.*, J. Feng, Effects of Fe-to-Co ratio on microstructure and mechanical properties of laser cladded FeCoCrBNiSi high-entropy alloy coatings, *Appl. Surf. Sci.* 450 (2018) 538–544. doi:10.1016/j.apsusc.2018.03.128.
47. S. Yin, *et al.*, The influence of aging temperature and aging time on the mechanical and tribological properties of selective laser melted maraging 18Ni-300 steel, *Addit. Manuf.* 22 (2018) 592–600. doi:10.1016/j.addma.2018.06.005.
48. K.I. Triantou, *et al*., Microstructure and tribological behavior of copper and composite copper+alumina cold sprayed coatings for various alumina contents, *Wear*. 336–337 (2015) 96–107. doi:10.1016/j.wear.2015.05.003.
49. S. Yin, *et al.*, Cold spraying of WC-Co-Ni coatings using porous WC-17Co powders: Formation mechanism, microstructure characterization and tribological performance, *Mater. Des.* 126 (2017) 305–313. doi:10.1016/j.matdes.2017.04.040.